JGR Space Physics

RESEARCH ARTICLE
10.1029/2025JA034905

Whistler Critical Mach Number Concept Revisited

Michael A. Balikhin[1], Oleksiy V. Agapitov[2], Vladimir Krasnoselskikh[3], Vadim Roytershteyn[4], Simon N. Walker[1], Michael Gedalin[5], Immanuel Christopher Jebaraj[6], and Lucas Colomban[2]

[1]ACSE, The University of Sheffield, Sheffield, UK, [2]Space Sciences Laboratory, University of California, Berkeley, CA, USA, [3]Laboratoire de Physique et Chimie de l'Environnement et de l'Espace, Orléans, France, [4]Space Sciences Institute, Boulder, CO, USA, [5]Department of Physics, Ben Gurion University of the Negev, Beer-Sheva, Israel, [6]Department of Physics and Astronomy, University of Turku, Turku, Finland

Abstract The formation of a collisionless shock is the result of a balance between nonlinear steepening and processes that counteract this steepening. Dispersive shocks are shocks in which dispersive processes counterbalance the front steepening and are formed when the dispersive spatial scale exceeds scales associated with resistive processes. Oblique dispersive shocks are characterized by a phase standing wave precursor adjacent to the magnetic ramp. The whistler critical Mach number M_{CrW} is defined as the maximum Mach number for which a linear whistler wave can phase stand upstream of the shock front. It was widely accepted that if the Mach number M exceeds M_{CrW}, linear whistler waves propagating along the shock normal are not able to "phase stand" in the upstream flow, and "…the shock will be initiated by a monotonic ramp." (Kennel et al., 1985, https://doi.org/10.1029/gm034p0001). In this study, we present results of numerical simulations and observations of shocks with $M > M_{CrW}$ that reveal the occurrence of an alternative scenario. For both the shock resulting from kinetic particle-in-cell simulations and that observed by MMS, the propagation direction of the precursor deviates from the shock normal direction. As a result, the velocity of the surface of constant phase along the shock normal exceeds the phase speed of these waves. It is shown that the propagation of the surface of constant phase along the shock normal occurs at a velocity that is nearly equal to the shock speed. Hence, these waves are "phase standing along the shock normal" in spite of $M > M_{CrW}$.

Key Points:

- Properties of wave precursors at the front of dispersive shocks are studied for cases when the whistler critical Mach M_{CrW} is exceeded
- It is shown that when the Mach number M is somewhat larger than M_{CrW} the propagation of the wave precursor deviates from the front normal n
- This precursor deviation enables the velocity of propagation of constant phase surfaces along n to be equal to the upstream speed even if $M > M_{CrW}$

Correspondence to:
O. V. Agapitov,
agapitov@ssl.berkeley.edu

Citation:
Balikhin, M. A., Agapitov, O. V., Krasnoselskikh, V., Roytershteyn, V., Walker, S. N., Gedalin, M., et al. (2026). Whistler critical Mach number concept revisited. *Journal of Geophysical Research: Space Physics*, *131*, e2025JA034905. https://doi.org/10.1029/2025JA034905

Received 1 DEC 2025
Accepted 22 DEC 2025

1. Introduction

Kennel et al. (1985) provides a thorough overview of the development of collisionless shock physics from the time when the very existence of such shocks was debated through two golden ages of collisionless shock physics to the state of this field during the culmination of the ISEE-1,2 missions. At this time it appeared that, at least for the range of parameters observed in the heliosphere, the study of collisionless shock physics was very close to achieving a comprehensive understanding of the physics involved. The classification of collisionless shocks according to the parameters of the upstream plasma flow had been developed, and an understanding of how the structure of observed shocks depended on these parameters has been reached. For weak shocks, it was recognized that the relation between the dispersive scale and the anomalous resistive spatial scale determines the transition between dispersive and resistive shocks. The concepts of the first M_{Cr1}, second M_{Cr2}, and whistler critical M_{CrW} Mach numbers had been developed. The evolution of shock structure with increasing Mach number, from subcritical, resistive (dispersive) shocks with Mach numbers below M_{Cr1} (M_{CrW}) to the supercritical reflective shocks with Mach numbers exceeding M_{Cr2} had been clearly understood. Data gained by the ISEE and AMPTE-UKS,IRM pairs of closely spaced satellites led to the conclusion that the actions of macroscopic fields at the quasi-perpendicular shock front can explain ion thermalization at the shock without invoking anomalous processes based on various micro-instabilities.

Toward the end of the ISEE-1,2 era it appeared that only a few problems related to the physics of heliospheric collisionless shocks remained unsolved. These included the "injection problem" and the problem of the third critical Mach number "above which ion reflection can not provide all the needed dissipation" (Kennel et al., 1985). However, modern, multi-spacecraft missions such as Cluster, THEMIS, and MMS have exposed many novel important aspects of the physics of collisionless shocks such as front non-stationarity and rippling or the role of small-scale structures within the shock front in the process of energy redistribution. Moreover, some features that were considered as well established toward the end of the ISEE era were reversed as result of these post-ISEE observations. One such example is the overshoot/undershoot structure downstream of the magnetic

ramp at the front of a supercritical quasi-perpendicular shock. It used to be considered as one of the flawless characteristics of supercritical reflection shocks, resulting from the joint gyration of the transmitted and initially reflected and later transmitted ion populations. Venus Express observations have shown that the overshoot/undershoot structure existed even for very weak sub-critical shocks (Balikhin et al., 2008). In the case of a low β weak shock, the gyration and drift motion of a single cold ion population led to variations in the kinematic pressure that, due to pressure balance, resulted in variations of the magnetic pressure and the magnitude of the magnetic field. In the current study, recent advanced numerical simulations and MMS observations of collisionless shocks are used to revisit another well-established concept, namely that of the whistler critical M_{CrW}.

The nature of a collisionless shock is determined by the processes that counterbalance the nonlinear steepening of the shock front (Sagdeev, 1960, 1962, 1966). If a particular set of physical processes can provide the required dissipation then the process associated with the longest spatial scale L_s defines the shock scale required to terminate the steepening process. For example, if for a weak shock, the spatial scale L_{is} corresponding to the anomalous resistivity process based on the ion-sound instability (Sagdeev, 1966) exceeds the spatial scales of other dissipative processes, the width of the shock front would be of the order L_{is}. In this case, anomalous resistivity based on the ion-sound instability will balance the shock nonlinearity and lead to the formation of resistive shock. Dispersive shocks, on the other hand are formed if the spatial scale that corresponds to wave dispersion exceeds spatial scales associated with resistive processes. In this case the process of the steepening of the shock front reaches the dispersion scale first.

Nonlinear steepening results from the nonlinear terms similar to the advection term $(\mathbf{V}\nabla)\,\mathbf{V}$. Steepening of the wave front can be represented as the generation of higher harmonics due to the nonlinearity (Sagdeev, 1966). For a monochromatic wave $A\exp i(\omega t - \mathbf{kr})$, advection will lead to the generation of the second harmonic $A_2\exp i(2\omega t - 2\mathbf{kr})$. If the wavelength of this second harmonic is sufficiently large, the MHD approximation will be valid to analyze its evolution. Since MHD waves are not dispersive, the phase velocity corresponding to the second harmonic will be the same as that of the original fundamental wave. Therefore the second harmonic wave will be at rest with respect to the front and its amplitude will increase due to the continuous transfer of energy from the original fundamental wave. At some point the second harmonic will be subjected to the same nonlinear processes leading to the generation of even higher harmonics, such as $A_4\exp i(4\omega t - 4\mathbf{kr})$ and so on. This cascade of energy transfer to shorter spatial scales will eventually reach scales that are too short for the MHD approximation to remain valid. At such short scales, the waves become dispersive since their phase velocity depends upon the spatial scales. These waves will propagate away from the shock front as their phase and group velocities differ from those of the original wave and stop any further steepening of the front. If the waves propagate along the normal to the shock front $\mathbf{n}$, the dependence of their phase velocity on spatial scales is determined by the angle θ_{Bn} between $\mathbf{n}$ and the upstream magnetic field $\mathbf{B}_{up}$. The critical angle θ^* can be defined as $\cos\theta^* = \sqrt{\frac{m_e}{M_i}}M_A$ where M_A is the Alfvén Mach number, M_i and m_e are ion and electron mass respectively (Kennel et al., 1985). For a perpendicular geometry ($\cos\theta_{Bn} > \cos\theta^*$), the wave phase velocity decreases with decreasing spatial scale (Kennel et al., 1985). In such a case the phase velocity of waves with shorter spatial scales generated in the process of shock front steepening will be smaller than the velocity of the shock front, forming a wave train downstream of the front. It is worth stating that the authors of the current study have never observed a shock with a downstream wave train. This is in agreement with the statement in Kennel et al. (1985) that "The trailing 90° electron inertial wave train has never been definitively identified in space." For oblique geometries ($\cos\theta_{Bn} < \cos\theta^*$), the phase velocity will increase with the decrease of the wave spatial scale, and a wave precursor will be formed upstream of the shock front. According to Karpman (1964) for a planar oblique dispersive shock an oscillatory wave precursor with wave vector parallel to $\mathbf{n}$ will develop. For a planar shock, if the upstream bulk velocity in the Normal Incident Frame does not exceed the maximum phase velocity of whistler waves, a wave precursor that is phase standing in the upstream flow is formed (Karpman, 1964). The upper limit of the fast magnetosonic Mach number for which a linear whistler wave can phase stand upstream of the front is referred to as whistler critical Mach number M_{CrW} (Kennel et al., 1985). The group velocity of whistler waves is about twice that of their phase velocity, which implies that when the Mach number moderately exceeds M_{CrW} these waves are still able to remove energy from the shock front even though they are unable to form a phase standing wave precursor.

The critical Mach numbers M_{Cr1}, M_{CrW}, and M_{Cr2} are used by Kennel et al. (1985) to describe the transition from a weak, subcritical, collisionless shock to a strong reflection shock. The first critical Mach number M_{Cr1} is defined

as the condition when the normal component of the downstream bulk plasma velocity is equal to the downstream sound speed (Kennel et al., 1985). The value of M_{Cr1} depends upon the upstream parameters and θ_{Bn}. If the Mach number exceeds M_{Cr1}, resistivity alone is not capable of providing the required dissipation (Coroniti, 1970; Kennel et al., 1985). For an oblique, dispersive shock, a stationary wave precursor with a wave vector along the shock normal can only be formed if the upstream Mach number does not exceed M_{CrW}. Obviously, the value of M_{CrW} also depends upon θ_{Bn} and other upstream parameters. Most of the time, the Mach numbers of planetary bow shocks in the heliosphere significantly exceed M_{Cr1} and M_{CrW}. Almost all bow shocks observed by space missions are ion-reflection shocks. In such shocks, the process of the reflection of a fraction of the incoming upstream ions provides the required dissipation at the shock front. The formation of an ion-reflection shock requires that a sufficient number of downstream ions are capable of reaching the shock front from downstream (Kennel et al., 1985). The corresponding condition is that the downstream plasma bulk velocity should be equal to the thermal velocity of ions (Kennel et al., 1985; Leroy et al., 1982). This condition defines the second critical Mach number M_{Cr2}. Ion reflection shocks form if the Mach number exceeds M_{Cr2}. The second critical Mach number exceeds M_{Cr1}. If the Mach number for a dissipative shock exceeds M_{Cr1} but is below M_{Cr2}, resistivity is not able to provide the entire dissipation required, but the shock is not strong enough to create an ion reflection shock. For dissipative shocks with a Mach number within the gap between M_{Cr1} and M_{Cr2}, some additional dissipation processes that can "assist" resistivity should occur. One of the widely accepted models for a possible additional dissipation process is based on the ion-sound subshock (Kennel et al., 1985; Manheimer & Spicer, 1985). The existence of shocks in the quasi-electrostatic subshock regime have been observed in laboratory (Eselevich et al., 1971) and space (Balikhin et al., 2002). Therefore, for dissipative shocks, it is evident that as the Mach number increases, the shock transforms from one based on pure resistivity to a shock with a subshock for which resistivity is assisted by "viscosity" to provide required dissipation and, with a further increase of Mach number, to the ion reflection shock.

The current study investigates the transformation of dispersive shocks with the increase of Mach number from below to above M_{CrW}. According to Kennel et al. (1985) if the Mach number exceeds the whistler critical Mach number, "a small amplitude whistler can not stand in the upstream flow and the shock will be initiated by a monotonic ramp with c/ω_{pe} scale length." (ω_{pe} is the electron plasma frequency).

This study proposes an alternative scenario for dispersive shocks with $M > M_{CrW}$. If the precursor's wave vector $\mathbf{k}$ direction deviates from the shock normal $\mathbf{n}$, the propagation of the surface of constant phase along the shock normal will increase by factor $\frac{1}{\cos\theta_{nk}}$, where θ_{nk} is the angle between $\mathbf{k}$ and $\mathbf{n}$. The alternative to the Kennel et al. (1985) scenario that "…the shock will be initiated by a monotonic ramp with c/ω_{pe} scale length." can be the formation of a whistler precursor like structure that propagates obliquely to the front normal such that the propagation of the surface of constant phase along the shock normal is equal to the Normal Incidence Frame (NIF) upstream velocity. In this paper, numerical simulations and in situ satellite observations that support such an alternative scenario are presented.

2. Simulations

In this section, particle-in-cell (PIC) numerical simulations are used to present a quasi-perpendicular shock that exhibits the alternative scenario explained in the introduction.

The numerical model of a quasi-perpendicular shock was performed using the fully kinetic PIC code VPIC (Bowers et al., 2008). The upstream plasma consists of two populations (ions and electrons) with isotropic Maxwellian distributions characterized by density n_0 and temperatures T_i and T_e chosen such that $\beta_e = 0.3$ and $\beta_i = 1$, where $\beta_s = 8\pi n_0 T_s/B_0^2$ $(s = i, e)$. The simulation is performed in a 2D domain of size $L_x \times L_y = (30 \times 5)d_i$, where $d_i = c/\omega_{pi}$ is the ion inertial length and $\omega_{ps} = \left(4\pi n_0 q_s^2/m_s\right)^{1/2}$. The ratio of the plasma frequency ω_{pe} to the cyclotron frequency ω_{ce} is 8. A uniform Cartesian grid of size 26544 × 4096 cells is used, such that the cell size is equal to the upstream Debye length $\lambda_d^2 = kT_e/4\pi n_0 e^2$. The computational particles have uniform and constant statistical weights, chosen such that the upstream density n_0 corresponds to 1,000 particles per cell per species. The time step is $\delta t\omega_{pe} \approx 0.027$.

The shock is created by the interaction of plasma flow injected from the $x = L_x$ boundary with the velocity $V_{inj} = -5.5V_A$ and the plasma reflected from the $x = 0$ boundary. Here, $V_A = B_0/\sqrt{4\pi n_0 m_i}$ is the Alfvén speed

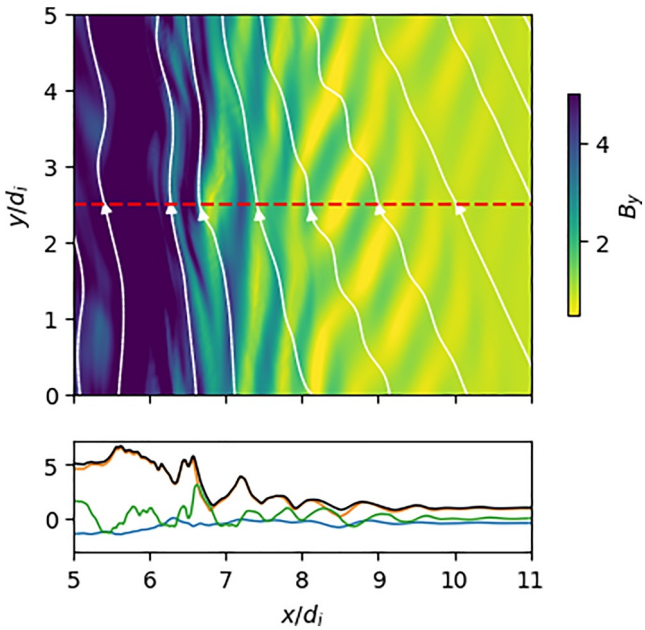

Figure 1. A slice of the simulation domain near the shock foot. The top panel shows B_y, while the bottom panel shows profiles of all three components B_j, $j = \{x, y, z\}$ of the magnetic field along a cut through the middle of the simulation domain, that is, $B_i(x, y = 2.5d_i)$.

defined with the upstream magnetic field B_0 and the density n_0. In the simulation frame of reference, the shock propagates in the positive x direction with the velocity $V_{sh} = 2V_A$. The upstream magnetic field is in the $x - y$ plane. The shock is characterized by the upstream Alfvén Mach number $M_A = V_0/V_A \approx 7.5$ and the angle between the shock normal and the magnetic field $\theta_{Bn} = 65°$. Here, V_0 is the upstream plasma speed. The compression ratios of magnetic field magnitude and plasma density are 4 ± 0.3 and 4.1 ± 0.3, respectively. $M_{Cr1} = 1.4, M_{Cr2} = 1.9, M_{CrW} \simeq 8.9$. A strong whistler precursor wave is observed upstream of the shock (Figure 1a). The amplitudes of this precursor are similar to the magnitude of the unperturbed magnetic field (Figure 1b). The wave normal is oblique to the background magnetic field $\theta_{Bk} = 40 \pm 2°$ and forms an angle $\theta_{nk} \simeq 25°$ with the shock normal.

The observed whistler wave phase speed $V_{ph}/V_A = M_W(\omega, \theta) = 6.7 \pm 0.4$ is lower than the shock speed ($M_W(\omega, \theta) < M_{CrW}$) and oblique to the shock normal. This supports the standing structure of the whistler precursor along the shock normal because $V_{ph\|} = \omega/k_x = V_{ph}/\cos\theta_{nk} \simeq 7.4\ M_A$. The phase of the whistler precursor propagates along the direction of the shock normal with about the same speed as the shock itself, and so is phase standing along the normal in the shock reference frame. Thus, the propagation of whistler waves leads to the formation of an oblique whistler precursor standing in the shock frame even for cases in which the Mach number doesn't exceed the critical whistler Mach number M_{CrW}, but exceeds $M_W(\omega, \theta)$.

3. Interplanetary Shock Observed by MMS on 8 January 2018

The interplanetary shock crossing by MMS considered here occurred on 8 January 2018, at 06:41 UT (Hanson et al., 2019; Hanson, Agapitov, Mozer, et al., 2020; Hanson, Agapitov, Vasko, et al., 2020). The magnitude of the magnetic field, plasma velocity, and ion density as measured by the MMS1 spacecraft are shown in Figure 2.

MMS mission was launched in 2015 and provides multipoint measurements from four closely spaced spacecraft (Burch et al., 2016). Measurements from the FGM magnetometer (Russell et al., 2016) magnetic field are used in the current study. The plasma parameters are based on fast plasma investigation suite (Pollock et al., 2016) data. Values of plasma velocity and density in the upstream and downstream regions, estimated by averaging over time intervals 06:26:56.8–06:36:46.3 UT and 06:26:56.8–06:50:07.3 respectively, were $n_{up} \approx 7.8\ cm^{-3}$, $n_{dw} \approx 17.2\ cm^{-3}$, $\mathbf{V}_{up} \approx [-291,9,\ -19]\ km/s$, and $\mathbf{V}_{dw} \approx [-339,5,\ -67]\ km/s$. The ion density increases at the shock front approximately 2.2 times, indicating a rather moderate Mach number. The compression ratio of the magnetic field magnitude is 2.3 ± 0.3, $M_{Cr1} = 1.2$, $M_{Cr2} = 1.7$, $M_{CrW} \simeq 8.9$. The profile of the magnetic field modulus does not exhibit a developed overshoot feature. Overshoot regions can be present both in supercritical ion reflection shocks (Kennel et al., 1985) and in subcritical low Mach shocks (Gedalin et al., 2015; Ofman et al., 2009). However, the absence of an overshoot indicates that the shock is not strong enough to be an ion reflection shock, and its Mach number is not much above the second critical Mach number M_{Cr2}. Timing of the front crossings by four MMS spacecraft has been used to identify the normal to the shock front $\mathbf{n}_t \approx [0.70, 0.01,\ -0.72]$ GSE, corresponding to $\theta_{Bn} \approx 64°$.

The value of the upstream magnetic field has been estimated by averaging over time intervals 06:41:1.7–06:41:4.2 UT: $\mathbf{B}_{up} = [-0.93,\ -4.06, 4.77]\ nT$. Figure 3 shows the three components and the magnitude of the magnetic field in the shock coordinate system in which the $\mathbf{n}_a$-axis is directed along the front normal $\mathbf{n}_t$, $\mathbf{l}_a$-axis lies along the projection of the upstream magnetic field into the plane orthogonal to the $\mathbf{n}_a$-axis, and the $\mathbf{m}_a$-axis completes the right-handed triad. It can be seen from this Figure that the spacecraft crossed the magnetic ramp around 06:41:11 UT. At the ramp, the magnitude of the magnetic field increases from about 4 nT to 12 nT. The absence of a significant change in the B_n component in the magnetic ramp region supports the identified normal to the shock front.

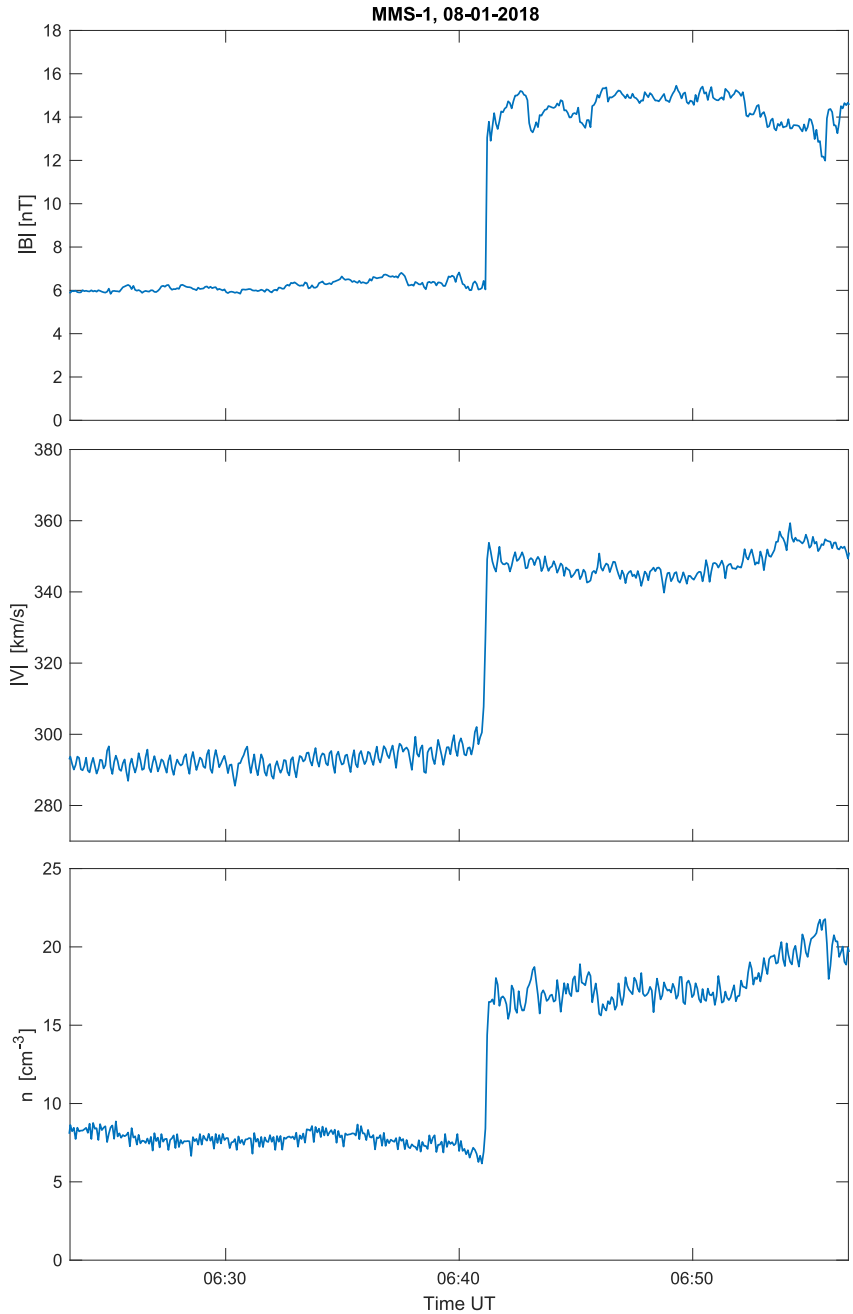

Figure 2. The magnitude of the magnetic field, plasma velocity, and density as observed by MMS1 during the interplanetary shock crossing on 8th of January 2018.

Conservation of ion flux across the shock front can be used to estimate the velocity of the shock front with respect to the spacecraft V_{sh}:

$$|V_{sh-flux}| = \left| \frac{n_{up} \cdot V^{\mathbf{n}}_{up} - n_{dw} \cdot V^{\mathbf{n}}_{dw}}{n_{dw} - n_{up}} \right| \approx 340\ km/s,$$

where $V^{\mathbf{n}}_{up} \approx 216.4\ km/s$ and $V^{\mathbf{n}}_{dw} \approx 283.8\ km/s$ are projections of the upstream and downstream velocities along the front normal $\mathbf{n}_t$. The velocity V_{sh} can also be estimated using the time difference for the shock detection by a pair of spacecraft. The choice of the spacecraft pair with the largest spacecraft separation along the shock

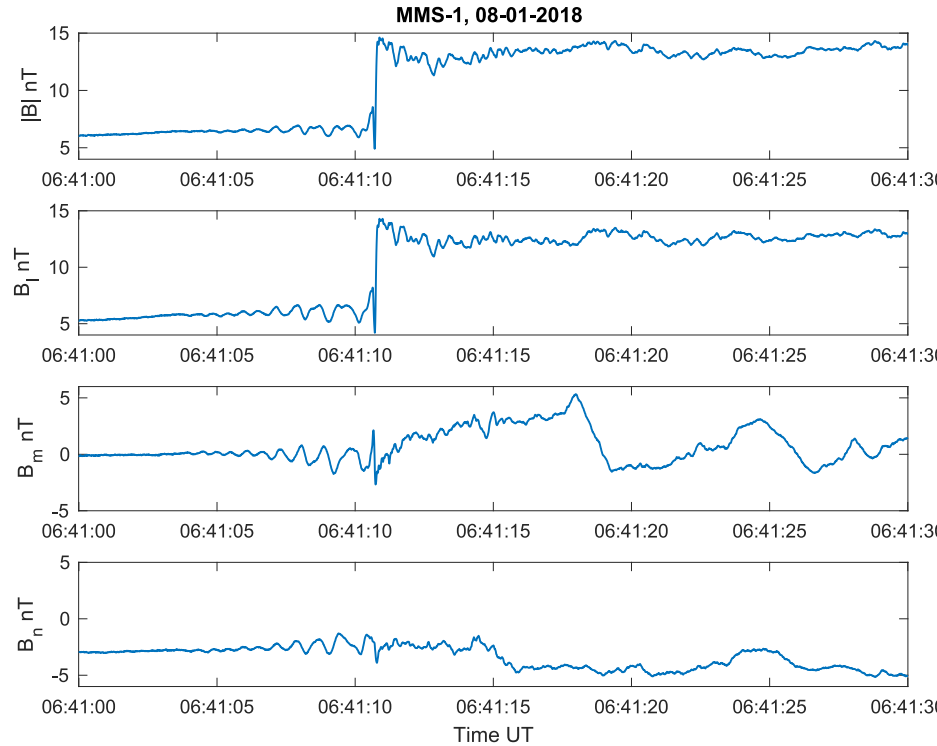

Figure 3. Three components and the magnitude of the magnetic field in the shock coordinate system based on $\mathbf{n}_{time}$ as observed by MMS1 during the interplanetary shock crossing on 8th of January 2018.

normal should reduce the possible error of such an estimate. Of the six possible combinations, the largest separation along the normal $\mathbf{n}_t$ direction corresponds to the MMS2 and MMS3 pair. The magnitude of the magnetic field as measured by MMS2 (red) and MMS3 (magenta) during the crossing of the magnetic ramp are shown in Figure 4. The separation vector between these two spacecraft during this crossing of the shock front is $[-5.0, 4.0, -14.8]$ km. Its projection along the normal $\mathbf{n}_t$ is ≈ 14.2 km. As can be seen from Figure 4 the time shift of the ramp observation between these two spacecraft is ≈ 0.0409 s, leading to the estimate of velocity as:

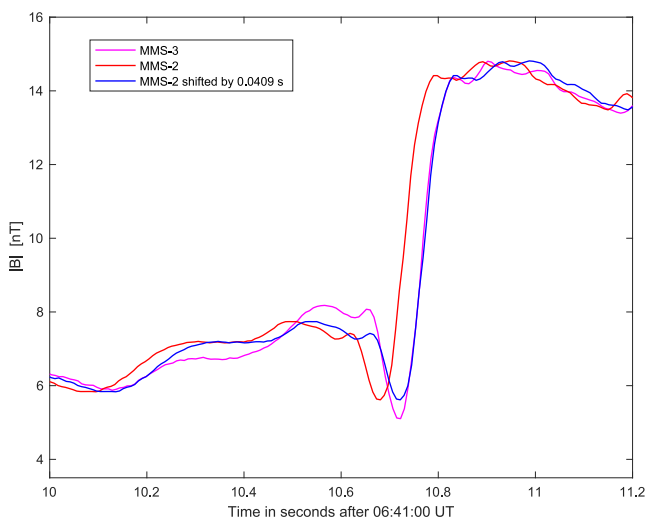

Figure 4. The magnitude of the magnetic field as measured by MMS2 (red) and MMS3 (magenta) during the crossing of the magnetic ramp. Blue line represents the magnitude of the magnetic field as measured by MMS2, but shifted by 0.0409 s.

$$|V_{sh}| = \left|\frac{14.2}{0.0409}\right| \approx 347\ km/s,$$

Both estimates for the shock-spacecraft velocity $V_{sh} = 347\ km/s$, and $V_{sh-flux} = 340\ km/s$, are very close, providing further support for the identified direction of the shock front normal. The value of V_{sh} will be used for further estimates in this work. The values of V_{sh}, $V^{\mathbf{n}}_{up}$, $\mathbf{B}_{up}$ and n_{up} result in an Alfvén velocity $V_A \approx 49\ km/s$ and an Alfvén Mach number $M_A \approx 2.6$.

A quasi-periodic wave precursor upstream of the magnetic ramp is evident in Figure 3 in all three components of the magnetic field B_l, B_m, and B_n. As this wave precursor is visible in the B_n component, its wave vector should differ from $\mathbf{n}_t$. The Minimum Variance method has been used to determine the direction of the wave vector for the precursor as measured by MMS-1, resulting in $\frac{\mathbf{k}}{|k|} \approx [0.05, -0.50, 0.86]$ GSE. The ratio of eigenvalues corresponding to minimum, intermediate, and maximum variance directions is 1:14.5:20.9, providing confidence in the identified direction of the wave vector. The angle between the wave vector and $\mathbf{n}_t$ is $\theta_{kn} \approx 48°$. Angles between the wave vector direction and satellite separation vectors are in the range from $\approx 17.5°$ (MMS1 and MMS2) to $\approx 70°$ (MMS3 and MMS4). The

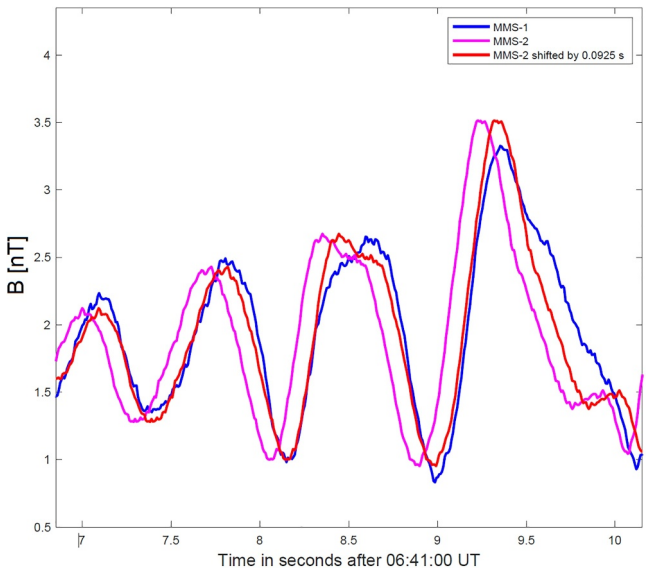

Figure 5. The components along the maximum variance direction of the magnetic field as measured by MMS2 (red) and MMS3 (magenta) during the crossing of the magnetic ramp. The blue curve represents the magnitude of the magnetic field as measured by MMS2 but shifted by 0.0409 s.

phase velocity of these waves can be estimated using the phase shift between observations of these waves by different spacecraft. Since the MMS1 and MMS2 separation makes the smallest angle with the identified direction of the wave vector, this pair has been used for the identification of the phase velocity. The Maximum Variance direction for the wave precursor, determined from MMS1 data, is $\mathbf{e}_{1Max} \approx [-0.998,\ -0.057, 0.030]$ GSE. Figure 5 displays $\mathbf{e}_{1Max}$ projection of the magnetic field for the wave precursor as measured by MMS1 (blue) and MMS2 (magenta). In addition, the same MMS2 component, but shifted by 0.0925 s, is displayed in the same figure (red). The closeness of blue and red lines allows an estimation of the phase velocity. The separation distance between these two spacecraft is $S_{21} \approx 24.2\ km$, therefore the phase velocity along the separation direction $V_{ph-sep} = \frac{S_{21}}{0.0925} \approx 262\ km/s$. The phase velocity along the wave vector in the spacecraft frame $V_{ph} = V_{ph-sep} \cdot \cos 17.5^\circ \approx 250\ km/s$ and along the shock normal $V_{ph-n} = \frac{V_{ph}}{\cos\theta_{kn}} \approx 373\ km/s$.

4. Discussion

The dispersion relation for whistler waves is given by

$$\omega = \Omega_{ce} \cos(\theta_{Bk}) k^2 c^2 / \omega_{pe}^2 \quad (1)$$

where Ω_{ce} and ω_{pe} are electron cyclotron and plasma frequencies correspondingly.

According to the dispersion relation for whistler waves propagating at the angle θ_{Bk} to the magnetic field (1), the frequency of the wave ω depends quadratically on the wave vector $\vec{k}$. From this dispersion, the wave group velocity $v_g = \frac{\partial\omega}{\partial k}$ exceeds its phase velocity $v_{ph} = \frac{\omega}{k}$ by a factor of 2. If the Mach number of a shock is between M_{CrW} and $2M_{CrW}$, the whistler waves with wave vector along the shock normal are unable to phase stand in the upstream but can still transport energy upstream, away from the shock front. The phase speed represents the velocity of propagation of the surface of constant phase along the wave vector. The velocity of the propagation of the surface of constant phase along the direction at angle θ_{ka} to the wave vector always exceeds v_{ph}: $v_{ph-a} = \frac{\omega}{k_a} = \frac{\omega}{k \cdot \cos\theta_{ka}}$. The velocity of the propagation of the surface of constant phase at some angle to **k** can exceed the maximum phase velocity of whistler waves along the wave normal. For a shock with Mach number $M > M_{CrW}$ the whistler wave packet that propagates at angle $A\cos\left(\frac{M_{CrW}}{M}\right)$ to the shock normal **n** will possess the velocity of propagation of the surface of constant phase along **n** equal to the speed of upstream flow V_{up} and could be considered "phase standing" along this direction. The condition for such a "phase standing" along the shock normal direction is that in the NIF frame V_{ph-n} should match the velocity of the upstream flow. For the in situ observations in the spacecraft frame V_{ph-n} should coincide with the shock velocity. For the PIC simulations presented above, the velocity of the propagation of the surface of constant phase along the shock normal is equal to 7.4 V_A, and its difference with the NIF upstream velocity $V_0 = 7.5\ V_A$ is ≈1.35%. However, it must be noted that the value of the upstream velocity V_0 is rather approximate.

For the interplanetary shock observed by MMS and discussed above, the values of V_{ph-n} and V_{sh} are also very close:

$$\frac{V_{ph-n} - V_{sh}}{V_{ph-n}} \approx 0.07.$$

Slight uncertainties in the estimates of experimental parameters could lead to such a small 7% discrepancy between V_{ph-n} and V_{sh}. For example, it could be explained by ≈4° error in the estimate of an angle between the wave vector and the shock normal.

Both in the PIC numerical simulations and in the shock observations presented above the directions of wave normals and the closeness of the shock velocity to the velocity of propagation of the surface of constant phase along **n** points to a wave precursor that propagates obliquely to **n** but is also "phase standing" along the normal direction. From classical one-dimensional theoretical models (e.g., Karpman, 1964) for whistler wave precursors, it was expected that their wave vector should be directed along the shock normal. In such a case, a phase standing precursor can only be formed if its Mach number is below the whistler critical Mach number M_{CrW}, following the concept that if the Mach number exceeds the whistler critical Mach number, as it was formulated in Kennel et al. (1985) "a small amplitude whistler can not stand in the upstream flow and the shock will be initiated by a monotonic ramp with c/ω_{pe} scale length" needs to be adjusted. The results from numerical simulations and observations point to the feasibility of this alternative scenario for Mach numbers moderately in excess of M_{CrW} (Section 2) or $M_W(\omega,\theta) < M_{CrW}$ (Section 3). In this alternative scenario, the direction of the precursor's wave vector deviates from the shock normal, enabling the whistler precursor to be "phase standing" along the front normal direction (up to extremely oblique values for supercritical shocks (Jebaraj et al., 2024)). The recognition that the critical whistler Mach number is effectively a function of θ_{Bn} (Kennel et al., 1985), so that $M_{CrW} \simeq 5$ is the factor that limits the frequency of the precursor existence and leads to oblique precursor propagation at much lower shock Mach numbers (as is the case discussed in Section 2 where $M_A = 7.5$ and $M_{CrW} \simeq 5$). An additional factor is the dependence of the whistler Mach number M_W on wave frequency. This leads to tending to oblique propagation even for the cases when $M_A < M_{CrW}$ but $M_W(\omega,\theta) < M_{CrW}$, and shocks nominally characterized as whistler-subcritical can develop oblique whistler precursors if the precursor frequency ω_w is such that $M_W(\omega,\theta) > 1$, the oblique propagation angle α and dispersion yield a favorable $M_W(\omega,\theta) * \cos(\alpha) = 1$, as was shown in the presented example in Section 3.

Conflict of Interest

The authors declare no conflicts of interest relevant to this study.

Data Availability Statement

The authors thank the entire MMS team for providing such excellent data, which are publicly available at: https://lasp.colorado.edu/mms/sdc/public/about/how-to/.

Acknowledgments
The authors acknowledge support from the International Space Science Institute, Bern, Switzerland. The simulations were performed using computational resources provided by the Texas Advanced Computing Center (TACC) at The University of Texas at Austin. MAB and SW were supported by the Science and Technology Facilities Council [ST/Y001575/1]. OVA, VK, and LC were supported by NASA Grants 80NSSC20K0697 and 80NSSC21K1770. OVA and LC were partially supported by NASA's Living with a Star (LWS) program (contract 80NSSC20K0218), and NASA Grants contracts 80NSSC22K0433 and 80NSSC22K0522. The work of VR was supported by NASA Grant 80NSSC21K1680. I.C.J. acknowledges support from the Research Council of Finland (X-Scale, Grant 371569).

References

Balikhin, M. A., Nozdrachev, M., Dunlop, M., Krasnoselskikh, V., Walker, S. N., Alleyne, H. S. K., et al. (2002). Observation of the terrestrial bow shock in quasi-electrostatic sub-shock regime. *Journal of Geophysical Research*, *107*(A8), 10. https://doi.org/10.1029/2001JA000327

Balikhin, M. A., Zhang, T. L., Gedalin, M., Ganushkina, N. Y., & Pope, S. A. (2008). Venus express observes a new type of shock with pure kinematic relaxation. *Geophysical Research Letters*, *35*(1), 1103. https://doi.org/10.1029/2007GL032495

Bowers, K. J., Albright, B. J., Yin, L., Bergen, B., & Kwan, T. J. T. (2008). Ultrahigh performance three-dimensional electromagnetic relativistic kinetic plasma simulation. *Physics of Plasmas*, *15*(5), 55703. https://doi.org/10.1063/1.2840133

Burch, J. L., Moore, T. E., Torbert, R. B., & Giles, B. L. (2016). Magnetospheric multiscale overview and science objectives. *Space Science Reviews*, *199*(1), 5–21. https://doi.org/10.1007/s11214-015-0164-9

Coroniti, F. V. (1970). Dissipation discontinuities in hydromagnetic shock waves. *Journal of Plasma Physics*, *4*(2), 265–282. https://doi.org/10.1017/S0022377800004992

Eselevich, V. G., Eskov, A. G., Kurtmullaev, R. C., & Malyutin, A. I. (1971). Isomagnetic discontinuity in a collisionless shock wave. *Soviet Physics Journal of Experimental and Theoretical Physics*, *33*, 1120.

Gedalin, M., Friedman, Y., & Balikhin, M. (2015). Collisionless relaxation of downstream ion distributions in low-mach number shocks. *Physics of Plasmas*, *22*(7), 072301. https://doi.org/10.1063/1.4926452

Hanson, E. L. M., Agapitov, O. V., Mozer, F. S., Krasnoselskikh, V., Bale, S. D., Avanov, L., et al. (2020). Terrestrial bow shock parameters from MMS measurements: Dependence on upstream and downstream time ranges. *Journal of Geophysical Research: Space Physics*, *125*(1), e2019JA027231. https://doi.org/10.1029/2019JA027231

Hanson, E. L. M., Agapitov, O. V., Mozer, F. S., Krasnoselskikh, V., Bale, S. D., Avanov, L., et al. (2019). Cross-shock potential in rippled versus planar quasi-perpendicular shocks observed by MMS. *Geophysical Research Letters*, *46*(5), 2381–2389. https://doi.org/10.1029/2018GL080240

Hanson, E. L. M., Agapitov, O. V., Vasko, I. Y., Mozer, F. S., Krasnoselskikh, V., Bale, S. D., et al. (2020). Shock drift acceleration of ions in an interplanetary shock observed by MMS. *The Astrophysical Journal*, *891*(1), L26. https://doi.org/10.3847/2041-8213/ab7761

Jebaraj, I. C., Agapitov, O., Krasnoselskikh, V., Vuorinen, L., Gedalin, M., Choi, K.-E., et al. (2024). Acceleration of electrons and ions by an AlmostAstrophysical shock in the heliosphere. *The Astrophysical Journal Letters*, *968*(1), L8. https://doi.org/10.3847/2041-8213/ad4daa

Karpman, V. I. (1964). Structure of the shock front propagating at an angle of the magnetic field in a low density plasma. *Soviet Physics–Technical Physics*, *8*, 715.

Kennel, C. F., Edmiston, J. P., & Hada, T. (1985). A quarter century of collisionless shock research. In R. G. Stone & B. T. Tsurutani (Eds.), *Collisionless shocks in the heliosphere: A tutorial review* (Vol. 34, pp. 1–36). American Geophysical Union. https://doi.org/10.1029/GM034p0001

Leroy, M. M., Winske, D., Goodrich, C. C., Wu, C. S., & Papadopoulos, K. (1982). The structure of perpendicular bow shocks. *Journal of Geophysical Research*, *87*(A7), 5081–5094. https://doi.org/10.1029/JA087iA07p05081

Manheimer, W. M., & Spicer, D. S. (1985). Longitudinal friction and intermediate mach number collisionless transverse magnetosonic shocks. *Physics of Plasmas*, *28*(2), 652–665. https://doi.org/10.1063/1.865408

Ofman, L., Balikhin, M., Russell, C. T., & Gedalin, M. (2009). Collisionless relaxation of ion distributions downstream of laminar quasi-perpendicular shocks. *Journal of Geophysical Research*, *114*(A9), 9106. https://doi.org/10.1029/2009JA014365

Pollock, C., Moore, T., Jacques, A., Burch, J., Gliese, U., Saito, Y., et al. (2016). Fast plasma investigation for magnetospheric multiscale. *Space Science Reviews*, *199*(1–4), 331–406. https://doi.org/10.1007/s11214-016-0245-4

Russell, C. T., Anderson, B. J., Baumjohann, W., Bromund, K. R., Dearborn, D., Fischer, D., et al. (2016). The magnetospheric multiscale magnetometers. *Space Science Reviews*, *199*(1–4), 189–256. https://doi.org/10.1007/s11214-014-0057-3

Sagdeev, R. Z. (1960). Non-linear motions of a rarefied plasma in a magnetic field. In M. A. Leontovich (Ed.), *Plasma physics and the problem of controlled thermonuclear reactions* (Vol. 4, pp. 454–460). Pergamon.

Sagdeev, R. Z. (1962). Fine structure of a shock-wave front propagated across a magnetic field in a rarefied plasma. *Soviet Physics - Technical Physics*, *6*(10), 867.

Sagdeev, R. Z. (1966). Cooperative phenomena and shock waves in collisionless plasmas. *Reviews of plasma physics*, *4*, 23.